Inorg. Chem. **2006**, *45*, 2251−2265

Electrochemistry and Spectroelectrochemistry of meso-Substituted Free-Base Corroles in Nonaqueous Media: Reactions of $(Cor)H_3$, $[(Cor)H_4]^+$, and $[(Cor)H_2]^-$

Jing Shen,[†] Jianguo Shao,[†,‡] Zhongping Ou,[†] Wenbo E,[†] Beata Koszarna,[§] Daniel T. Gryko,*[,§] and Karl M. Kadish*[,†]

Department of Chemistry, University of Houston, Houston, Texas 77204-5003, and Institute of Organic Chemistry, Polish Academy of Science, Kasprzaka 44/52, 01-224 Warsaw, Poland

Received October 6, 2005

Eleven free-base corroles with different electron-donating or electron-withdrawing meso substituents were characterized as to their electrochemistry and UV–visible spectroscopy in benzonitrile (PhCN) or pyridine containing tetra-*n*-butylammonium perchlorate (0.1 M). Six forms of the compounds with different numbers of protons and/or oxidation states were spectroscopically identified and are represented as $(Cor)H_3$, $(^{\bullet}Cor)H_2$, $[(Cor)H_2]^-$, $[(^{\bullet}Cor)H_2]^{2-}$, $[(Cor)H_4]^+$, and $[(^{\bullet}Cor)H_4]^{2+}$, where Cor is a trianionic corrole macrocycle. The electrochemistry and UV–visible properties are a function of corrole basicity, solvent basicity, and types or sizes of the meso substituents, and the compounds could be subdivided into one of two different groups, one of which comprises sterically hindered corroles and another that does not. The electroactive species in PhCN is $(Cor)H_3$, whereas in pyridine, one inner proton dissociates, generating a mixture of $(Cor)H_3$, $[(Cor)H_2]^-$, and pyH^+. The addition of one electron to $[(Cor)H_2]^-$ reversibly gives the $[(^{\bullet}Cor)H_2]^{2-}$ π-anion radical, whereas a reversible oxidation of the same species gives the neutral radical $(^{\bullet}Cor)H_2$. The first one-electron reduction of $(Cor)H_3$ occurs at the macrocycle in PhCN, but the initial product rapidly converts to $[(Cor)H_2]^-$, which undergoes additional reversible redox reactions at the conjugated π-ring system. The first oxidation of $(Cor)H_3$ in PhCN leads to a mixture of $(^{\bullet}Cor)H_2$ and $[(Cor)H_4]^+$, both of which could be further oxidized or reduced. The UV–visible spectra of $[(Cor)H_4]^+$ were measured in PhCN after titrations with trifluoroacetic acid, after which selected samples were examined as to their electrochemistry. The HOMO–LUMO gaps of $[(Cor)H_2]^-$, $(Cor)H_3$, and $[(Cor)H_4]^+$ were also determined.

Introduction

Research activity on metallocorroles has increased dramatically in recent years, providing much information on how these compounds differ from related metalloporphyrins.[1−4] Numerous transition-metal and main-group metallocorroles have been synthesized and spectroscopically or electrochemically characterized in nonaqueous media,[1−4] but relatively few studies have concentrated on unmetalated free-base corrole precursors, in large part because these species undergo a facile gain or loss of protons, giving a mixture of the neutral corrole, either protonated $[(Cor)H_4]^+$ or deprotonated $[(Cor)H_2]^-$. (Cor represents the trianionic macrocycle in the absence of protons.[5−11])

* To whom correspondence should be addressed. E-mail: kkadish@uh.edu (K.M.K.); danieltgryko@lycos.com (D.T.G).

[†] University of Houston.

[‡] Currently with Department of Chemistry, Midwestern State University, Wichita Falls, TX 76308.

[§] Polish Academy of Science.

(1) Paolesse, R. In *The Porphyrin Handbook*; Kadish, K. M., Smith, K. M., Guilard, R., Eds.; Academic Press: San Diego, CA, 2000; Vol. 2, pp 201−232.

(2) Erben, C.; Will, S.; Kadish, K. M. In *The Porphyrin Handbook*; Kadish, K. M., Smith, K. M., Guilard, R., Eds.; Academic Press: San Diego, CA, 2000; Vol. 2, pp 233−300.

(3) Guilard, R.; Barbe, J.-M.; Stern, C.; Kadish, K. M. In *The Porphyrin Handbook*; Kadish, K. M., Smith, K. M., Guilard, R., Eds.; Elsevier: San Diego, CA, 2003; Vol. 18, pp 303−349.

(4) Gryko, D. T.; Fox, J. P.; Goldberg, D. P. *J. Porphyrins Phthalocyanines* **2004**, *8*, 1091−1105.

(5) Paolesse, R.; Jaquinod, L.; Nurco, D. J.; Mini, S.; Sagone, F.; Boschi, T.; Smith, K. M. *Chem. Commun.* **1999**, *14*, 1307−1308.

(6) Johnson, A. W.; Kay, I. T. *J. Chem. Soc.* **1965**, 1620−1629.

(7) Broadhurst, M. J.; Grigg, R.; Johnson, A. W.; Shelton, G. *J. Chem. Soc., Perkin Trans. 1* **1972**, *1*, 143−151.

(8) Grigg, R.; Hamilton, R. J.; Jozefowicz, M. L.; Rochester, C. H.; Terrel, R. J.; Wickwar, H. J. *J. Chem. Soc., Perkin Trans. 2* **1973**, *4*, 407−413.

(9) Endeward, B.; Plato, M.; Will, S.; Vogel, E.; Szycewski, A.; Mobius, K. *Appl. Magn. Reson.* **1998**, *14*, 69−80.

(10) Gross, Z.; Galili, N.; Saltsman, I. *Angew. Chem., Int. Ed.* **1999**, *38*, 1427−1429.

10.1021/ic051729h CCC: $33.50
Published on Web 02/01/2006

Scheme 1

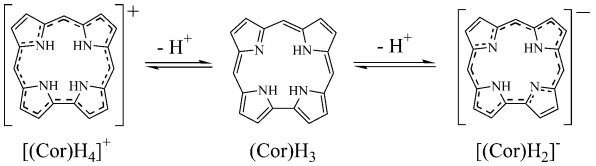

The addition or loss of protons by $(Cor)H_3$ occurs at the four inner nitrogens of the macrocycle, as shown in Scheme 1, with the exact position of the acid/base equilibria being determined by the relative basicity of the solvent and corrole, where the latter can be tuned by the systematic placement of electron-donating or electron-withdrawing substituents at the meso- or β-pyrrole positions of the macrocycle.[12−15] In addition, acidic solvents containing $(Cor)H_3$ generally lead to $[(Cor)H_4]^+$, whereas basic solvents generally lead to $[(Cor)H_2]^-$, as can be ascertained by an analysis of the UV−visible spectra that show a strong Q band for both the protonated and deprotonated forms of the free-base corroles but not for the neutral compounds.[1,2]

One of our own interests in metallocorroles has been in evaluating the redox potentials and UV−visible spectroscopic properties of these complexes in their oxidized or reduced forms using thin-layer spectroelectrochemistry and then comparing these data to those of related metalloporphyrins to better understand the chemical reactivity of the examined metallocorroles[3,12,16−18] and related corrolazines.[19] In this regard, it is also important to evaluate the electrochemistry and spectroelectrochemistry of the free-base corroles and to know how the redox potentials and UV−visible spectra will change as one adds or abstracts protons at the four central nitrogen atoms of the macrocycle, that is, upon going from $(Cor)H_3$ to $[(Cor)H_2]^-$ or from $(Cor)H_3$ to $[(Cor)H_4]^+$. We know from the literature that $[(OEC)H_4]^+$ (where OEC = octaethylcorrole) can be oxidized or reduced in nonaqueous media,[20] but we do not know anything about the electrochemistry of deprotonated $[(Cor)H_2]^-$ derivatives or even neutral corroles of the form $(Cor)H_3$. This is investigated in the present Article, which reports the electrochemistry and UV−visible spectroscopy of 11 different free-base corroles in their neutral, protonated, and deprotonated forms. The structures of the investigated compounds are shown in Charts 1 and 2 and arranged according to the corrole substitution pattern at the three meso positions of the macrocycle giving either *trans*-A_2B or A_3 complexes. Electrochemistry combined with UV−visible spectroelectrochemistry is used

Chart 1

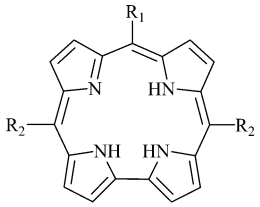

(A_2B-corrole)

compound	R_1	R_2	$\Sigma\sigma^a$	group type
2	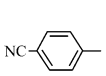	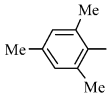	-0.36	B
3		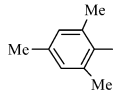	b	B
5		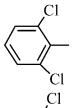	b	B
6	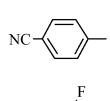	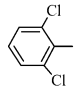	1.46	B
8			b	A

[a] Individual σ values were taken from ref 30 and are based on substituents at the ortho, para, and meta positions of the meso-phenyl groups. [b]Sigma values are not available for compounds with pyridyl groups at the meso-position of the corrole.

Chart 2

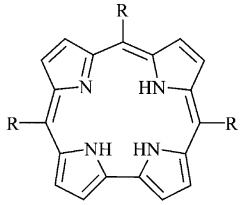

(A_3-corrole)

compound	R	$\Sigma\sigma^a$	group type	compound	R	$\Sigma\sigma^a$	group type
1		-0.51	A	**9**		2.58	A
4		1.62	A	**10**		3.72	B
7		1.68	A	**11**		3.66	B

[a] Individual σ values were taken from ref 30 and are based on substituents at the ortho, para, and meta positions of the meso-phenyl groups.

(11) Mahammed, A.; Weaver, J. J.; Gray, H. B.; Abdelas, M.; Gross, Z. *Tetrahedron Lett.* **2003**, *44*, 2077−2079.
(12) Ou, Z.; Shao, J.; Zhao, H.; Ohkubo, K.; Washbotten, I. H.; Fukuzumi, S.; Ghosh, A.; Kadish, K. M. *J. Porphyrins Phthalocyanines* **2004**, *8*, 1236−1247.
(13) Adamian, V.; D'Souza, F.; Licoccia, S.; Di Vona, M. L.; Tassoni, E.; Paolesse, R.; Boschi, T.; Kadish, K. M. *Inorg. Chem.* **1995**, *34*, 532−540.
(14) Steene, E.; Dey, A.; Ghosh, A. *J. Am. Chem. Soc.* **2003**, *125*, 16300−16309.
(15) Ghosh, A.; Steene, E. *J. Inorg. Biochem.* **2002**, *91*, 423−436.
(16) Guilard, R.; Gros, C. P.; Barbe, J.-M.; Espinosa, E.; Jerome, F.; Tabard, A.; Latour, J.-M.; Shao, J.; Ou, Z.; Kadish, K. M. *Inorg. Chem.* **2004**, *4323*, 7441−7455.
(17) Kadish, K. M.; Ou, Z.; Shao, J.; Gros, C. P.; Barbe, J.-M.; Jerome, F.; Bolze, F.; Burdet, F.; Guilard, R. *Inorg. Chem.* **2002**, *41*, 3990−4005.
(18) Kadish, K. M.; Shao, J.; Ou, Z.; Gros, C. P.; Bolze, F.; Barbe, J.-M.; Guilard, R. *Inorg. Chem.* **2003**, *42*, 4062−4070.
(19) Lansky, D. E.; Mandimutsira, B.; Ramdhanie, B.; Clausen, M.; Penner-Hahn, J.; Zvyagin, S. A.; Telser, J.; Krzystek, J.; Zhan, R.; Ou, Z.; Kadish, K. M.; Zakharov, L.; Rheingold, A. L.; Goldberg, D. P. *Inorg. Chem.* **2005**, *44*, 4485−4498.
(20) Gisselbrecht, J.-P.; Gross, M.; Vogel, E.; Will, S. *J. Electroanal. Chem.* **2001**, *505*, 170−172.

to elucidate the electrooxidation and electroreduction mechanisms, half-wave potentials, and UV−visible spectra for a variety of in situ-generated free-base corroles that have never before been spectroscopically characterized. The numbering of the compounds from **1** to **11** in Charts 1 and 2 is based on the first oxidation potential of $[(Cor)H_2]^-$ in pyridine, whereas group types A and B are based on the UV−visible spectra of the neutral free-base corroles in PhCN, where two different types of spectral patterns are observed depending upon the type and size of the meso substituents on the macrocycle. Both of these points will be discussed in this article. The compounds in group B can be considered to be sterically hindered corroles on the basis of comparisons with related porphyrins,[21] whereas those in group A can be considered to be nonsterically hindered derivatives.

As will be discussed, the judicious selection of solvent conditions enables a facile generation of pure samples of $[(Cor)H_2]^-$, $[(Cor)H_4]^+$, or $(^{\bullet}Cor)H_2$ in solution, and these different forms of the free-base corroles can be oxidized or reduced for comparison with data on the initial $(Cor)H_3$ derivatives and also analyzed as a function of the type of substituent at the meso position of the macrocycle.

Experimental Section

Instrumentation. Cyclic voltammetry was carried out with an EG&G model 173 potentiostat. A three-electrode system was used and consisted of a platinum-disk working electrode, a platinum wire counter electrode, and a saturated calomel reference electrode (SCE). The SCE was separated from the bulk of the solution by a fritted-glass bridge of low porosity that contained the solvent/supporting electrolyte mixture. All potentials are referenced to the SCE.

UV−visible spectroelectrochemical experiments were performed with an optically transparent platinum thin-layer electrode of the type described in the literature.[22] Potentials were applied with an EG&G model 173 potentiostat. Time-resolved UV−visible spectra were recorded with a Hewlett-Packard model 8453 diode array rapid-scanning spectrophotometer.

Chemicals and Reagents. The investigated compounds were synthesized as described in the literature: **1**,[23] **2**,[24] **3**,[25] **4**,[23] **5**,[25] **6**,[23] **7**,[23] **8**,[25] and **9**−**11**.[23] The structures are given in Charts 1 and 2, which differ according to the substitution pattern at the meso positions of the macrocycle, one group of compounds being *trans*-A_2B-type derivatives (cpds **2**, **3**, **5**, **6**, and **8**) and the other being A_3-type complexes (cpds **1**, **4**, **7**, and **9**−**11**). Pyridine (py, 99.8%) was obtained from Sigma-Aldrich and used as received. Benzonitrile (PhCN) was purchased from Aldrich and distilled over P_2O_5 under vacuum prior to use. Tetra-*n*-butylammonium perchlorate (TBAP, Fluka chemical company) was twice recrystallized from absolute ethanol and dried in a vacuum oven at 40 °C for a week before use. Trifluoroacetic acid (TFA, 99+%) was purchased from Aldrich and used as received.

Results and Discussion

Rationale for Design and Synthesis. In our initial studies of triaryl free-base corroles, we observed that the color and UV−visible spectra of the neutral compounds seemed to depend on the presence or absence of a substituent at one or both of the ortho positions of the meso-substituted phenyl groups. Differences had previously been observed in the NMR spectra of the compounds, some of which were broad and others of which were sharp, depending upon the steric hindrance of the corrole.[23−25] This suggested to us that a truly comprehensive study on the electrochemistry of free-base corroles should involve not only a broad set of compounds possessing different types of substituents but also derivatives that were sterically hindered and those that were nonsterically hindered.

To accomplish our goal, we elected to examine meso-substituted corroles with two substitution patterns: A_3-type derivatives, compounds **1**, **4**, **7**, and **9**−**11**, and *trans*-A_2B-type derivatives, compounds **2**, **3**, **5**, **6** and **8** (Charts 1 and 2). The A_3-corroles were synthesized directly from aldehydes and pyrrole,[23] and the *trans*-A_2B-corroles were synthesized via dipyrromethanes.[23−25] We have chosen for characterization compounds bearing electron-donating and electron-withdrawing substituents as well as corroles having pyridyl substituents that have never before been studied in detail. Altogether, 11 different free-base corroles are characterized, 6 of which can be considered to be sterically hindered (group B).

Electrochemistry in Pyridine and Electroreduction in PhCN. The electrochemistry of the free-base corroles in nonaqueous media was found to be a function of the corrole meso substituents as well as the specific nonaqueous solvent, which in this case was PhCN or pyridine. As will be discussed, $(Cor)H_3$ is the electroactive form of the corrole in PhCN containing 0.1 M TBAP; however, in pyridine, dissociation of one inner proton from the corrole readily occurs to generate $[(Cor)H_2]^-$ and H^+, as shown in eq 1. The liberated proton then reacts with pyridine to give pyH^+, which is also electroactive as discussed in the following paragraphs.

$$(Cor)H_3 \rightleftharpoons [(Cor)H_2]^- + H^+ \qquad (1)$$

Examples of cyclic voltammograms for the reduction and oxidation of $[((CF_3)_2Ph)_3Cor]H_3$ (**9**) at a Pt electrode in pyridine and PhCN are shown in Figure 1a, and a summary of the redox potentials for all of the compounds in the two solvents is given in Table 1, where the justification for the assignment of each reactant to a specific electroactive species, $(Cor)H_3$, $[(Cor)H_2]^-$, or pyH^+, is given in the following paragraphs.

The electrochemistry of **9** at a Pt electrode in pyridine consists of three reductions and two oxidations between +0.9 and −2.0 V versus SCE. The first reduction is irreversible and is located at a peak potential of −0.64 V for a scan rate of 0.1 V/s. Two additional reversible reductions located at $E_{1/2} = -1.52$ and −1.86 V are observed for this compound. The first oxidation of **9** is also reversible in pyridine and is located at 0.27 V, and this process is followed by an additional irreversible oxidation at $E_p = 0.84$ V, which is just on the edge of the solvent potential window.

(21) Lindsey, J. S.; Wagner, R. W. *J. Org. Chem.* **1989**, *54*, 828−836.
(22) Lin, X. Q.; Kadish, K. M. *Anal. Chem.* **1985**, *57*, 1498−1501.
(23) Gryko, D. T.; Koszarna, B. *Org. Biomol. Chem.* **2003**, *1*, 350−357.
(24) Gryko, D. T.; Jadach, K. *J. Org. Chem.* **2001**, *66*, 4267−4275.
(25) Gryko, D. T.; Piechota, K. E. *J. Porphyrins Phthalocyanines* **2002**, *6*, 81−97.

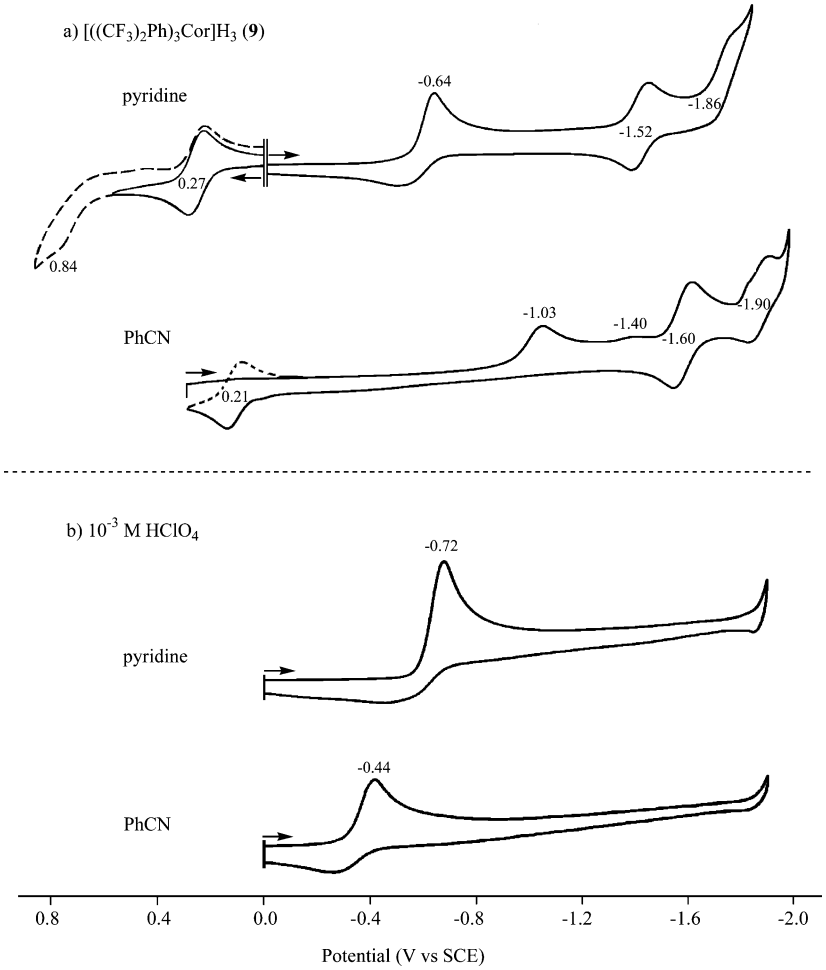

Figure 1. Cyclic voltammograms of (a) $[((CF_3)_2Ph)_3Cor]H_3$ (**9**) and (b) $HClO_4$ (10^{-3} M) in pyridine and PhCN, 0.1 M TBAP. Scan rate: 0.1 V/s.

Table 1. Half-Wave Potentials (V vs SCE) at a Pt Electrode in Pyridine and PhCN Containing 0.1 M TBAP

		$[(Cor)H_2]^-$ ox			$(Cor)H_3$ red[a]		$[(Cor)H_2]^-$ red	
solv.	compound	second[a]	first	pyH^+ red[a]	first	second	first	second
py	$[(MePh)_3Cor]H_3$ (**1**)	0.54	0.10	−0.80			−1.85	
	$[(Me_3Ph)_2(CNPh)Cor]H_3$ (**2**)	0.68	0.13	−0.79			−1.96	
	$[(Me_3Ph)_2(py)Cor]H_3$ (**3**)	0.69	0.14	−0.79			−1.93	
	$[(CF_3Ph)_3Cor]H_3$ (**4**)	0.70	0.18	−0.70			−1.67	
	$[(Cl_2Ph)_2(py)Cor]H_3$ (**5**)	0.76	0.22	−0.74			−1.80	
	$[(Cl_2Ph)_2(CNPh)Cor]H_3$ (**6**)	0.75	0.21	−0.73			−1.78	
	$[(CNPh)_3Cor]H_3$ (**7**)	0.70	0.20	−0.68			−1.65	
	$[(py)_2(F_2Ph)Cor]H_3$ (**8**)	0.72	0.24	−0.69			−1.62	−1.94[a]
	$[((CF_3)_2Ph)_3Cor]H_3$ (**9**)	0.84	0.27	−0.64			−1.52	−1.86
	$[(F_4N_3Ph)_3Cor]H_3$ (**10**)	0.82	0.34	−0.65			−1.64[a]	
	$[(F_5Ph)_3Cor]H_3$ (**11**)	0.84	0.37	−0.65			−1.57	
PhCN	$[(MePh)_3Cor]H_3$ (**1**)		−0.08		−1.36		−1.91	
	$[(Me_3Ph)_2(CNPh)Cor]H_3$ (**2**)		−0.02		−1.30	−1.54		
	$[(Me_3Ph)_2(py)Cor]H_3$ (**3**)		−0.02		−1.33			
	$[(CF_3Ph)_3Cor]H_3$ (**4**)		0.09		−1.13	−1.50	−1.71	
	$[(Cl_2Ph)_2(py)Cor]H_3$ (**5**)		0.09		−1.21		−1.86	
	$[(Cl_2Ph)_2(CNPh)Cor]H_3$ (**6**)		0.10		−1.23	−1.53	−1.85	
	$[(CNPh)_3Cor]H_3$ (**7**)		0.11		−1.13	−1.53	−1.72	
	$[(py)_2(F_2Ph)Cor]H_3$ (**8**)		0.14		−0.98		−1.67	−1.98[a]
	$[((CF_3)_2Ph)_3Cor]H_3$ (**9**)		0.21		−1.03	−1.40	−1.60	−1.90
	$[(F_4N_3Ph)_3Cor]H_3$ (**10**)		0.30		−1.02	−1.56[b]	−1.82[b]	
	$[(F_5Ph)_3Cor]H_3$ (**11**)		0.31		−1.04	−1.55	−1.64	

[a] Peak potential at a scan rate of 0.1 V/s. [b] The process overlapped with the reduction of the azide group on the corrole.

Some of the features of the voltammogram in pyridine are also observed for compound **9** in PhCN, but differences do exist. One difference is in the potential of the first reduction that is located at $E_p = -1.03$ V in PhCN as compared to that at $E_p = -0.64$ V in pyridine. Another is the presence of an irreversible process with reduced intensity at $E_p = -1.40$ V in PhCN that is not seen in pyridine. In addition, compound **9** shows no redox processes in PhCN

between 0.00 and 0.35 V on initial scans in a positive direction, but a well-defined oxidation/reduction couple is seen on the second positive potential sweep after scanning through the first reduction. This is shown in Figure 1a where the new redox couple is located at $E_{1/2} = 0.21$ V.

The redox potentials and shapes of the current−voltage curves for the other 10 investigated corroles are similar to those of compound **9** in the two solvents, and in each case, distinct differences are observed between pyridine and PhCN. For example, all of the voltammograms in pyridine display an irreversible first reduction at $E_p = -0.65$ to -0.80 V, whereas PhCN solutions of the same compounds display an irreversible first reduction at $E_p = -0.98$ to -1.36 V (Table 1). Some of the voltammograms also exhibit an irreversible reduction with reduced current at $E_p = -1.40$ to -1.56 V in PhCN, but none of the corroles show this reduction in pyridine (Figure 1 for **9**). In addition, all of the compounds exhibit one or two reversible reductions between -1.52 and -1.96 V. The exact value of $E_{1/2}$ for the latter processes depends on the specific corrole, but very little difference in $E_{1/2}$ is observed between the two solvents for a given compound. Another point of similarity involves the first oxidation in pyridine. The reversible potentials range from $E_{1/2} = 0.10$ to 0.37 V for the 11 compounds in pyridine, and a similar redox couple is observed for $(Cor)H_3$ in PhCN after sweeping the potential to values of negative E_p for the first reduction. An example of this behavior is shown in Figure 1 for the case of compound **9**, where $E_{1/2}$ for the oxidation and rereduction of the electrogenerated species is 0.21 V.

As indicated in eq 1, the proton dissociation of $(Cor)H_3$ in pyridine leads to $[(Cor)H_2]^-$ and H^+ (pyH^+), the latter of which is reduced to H_2, giving back the initial pyridine solvent. The potential for H^+ reduction in nonaqueous media depends on the concentration of the acid in solution, the properties of the nonaqueous solvent, and the type of working electrode material.[26,27] Of most importance in the current study is the fact that a pyridine solution to which has been added 10^{-3} M $HClO_4$ and 0.1 M TBAP exhibits an irreversible proton reduction at $E_p = -0.72$ V in pyridine and -0.44 V in PhCN for a scan rate of 0.1 V/s (Figure 1b). The peak potential for the irreversible reduction of the added proton in pyridine is just in the range of E_p for a similar process for all 11 free-base corroles in this solvent (-0.65 to -0.80 V). The shapes of the current−voltage curves are also similar, thus strongly suggesting a reduction of pyH^+ after the loss of one proton from $(Cor)H_3$, as shown in eq 1. Proton reduction is not seen at a Pt electrode for PhCN solutions containing either $[((CF_3)_2Ph)_3Cor]H_3$ (**9**) or any of the other free-base corroles, where 10^{-3} M $HClO_4$ displays a reduction peak at $E_p = -0.44$ V (Figure 1b). This result is consistent with the equilibrium in eq 1 being shifted completely toward the undissociated form of $(Cor)H_3$ in PhCN, a conclusion also reached on the basis of the UV−visible spectra for the initial compound, which shows no evidence for $[(Cor)H_2]^-$ under these solution conditions.

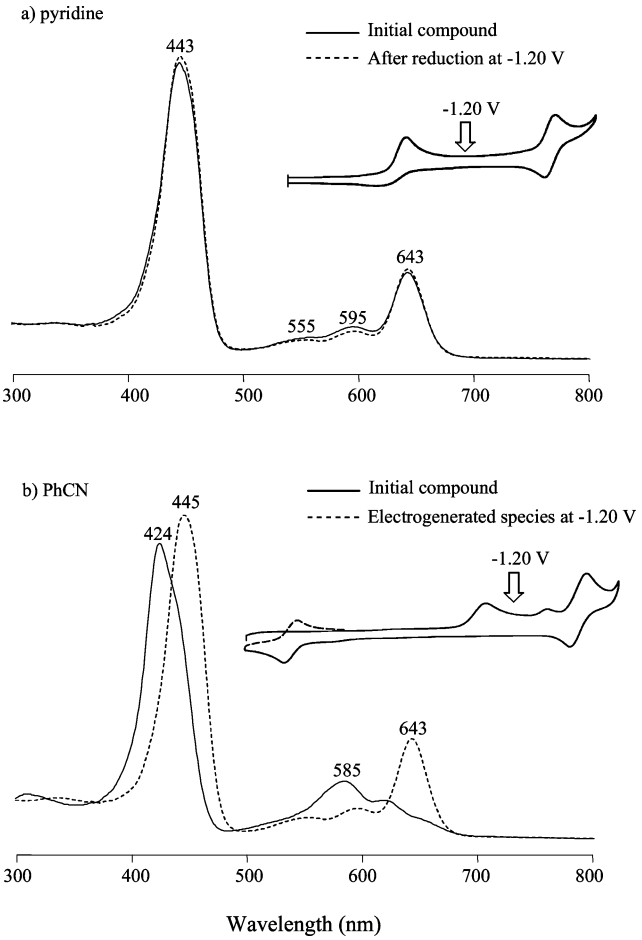

Figure 2. Thin-layer UV−visible spectra of $[((CF_3)_2Ph)_3Cor]H_3$ (**9**) before (−) and after (- - -) electroreduction in (a) pyridine and (b) PhCN, 0.1 M TBAP.

An assignment of the actual corrole in solution before carrying out the electrochemical experiments, $(Cor)H_3$ or $[(Cor)H_2]^-$, can also be made on the basis of the electrochemistry combined with the UV−visible spectroscopic characterization of the reactant and product after controlled-potential oxidation or reduction in a thin-layer cell. The voltammetric data in Figure 1 suggest that the first irreversible reduction in PhCN involves electron addition to $[((CF_3)_2Ph)_3Cor]H_3$ (**9**) rather than the reduction of a liberated H^+ in solution, and this is also the conclusion arrived at from an analysis of the thin-layer spectra shown in Figure 2. As seen in this Figure, the UV−visible spectra in pyridine are virtually identical before (−) and after (- - -) the controlled-potential reduction of the proton (pyH^+) from $[((CF_3)_2Ph)_3Cor]H_3$ (**9**), and this is what would be expected for the dissociation shown in eq 1 if it were completely to the right, that is, if all of the $(Cor)H_3$ were converted to $[(Cor)H_2]^-$.

In contrast, quite different UV−visible spectra are obtained in PhCN before (−) and after (- - -) a controlled-potential reduction at -1.20 V. Here, the undissociated $[((CF_3)_2Ph)_3Cor]H_3$ (**9**) is characterized by a Soret band at 424 nm, a shoulder at 442 nm, and two visible bands at 585 and 620 nm. This contrasts with the spectrum after electroreduction

(26) Sawyer, D. T.; Sobkowiak, A.; Roberts, J. L., Jr. *Electrochemistry for Chemists*, 2nd Ed.; John Wiley & Sons: New York, 1995.
(27) Barrette, W. C., Jr.; Johnson, H. W., Jr.; Sawyer, D. T. *Anal. Chem.* **1984**, *56*, 1890−1898.

in PhCN. The new spectrum has a Soret band at 445 nm and an intense visible band at 643 nm, which is virtually the same spectral pattern seen for **9** in pyridine before and after the controlled-potential reduction of the liberated H^+ (pyH^+) from $(Cor)H_3$.

The spectroelectrochemistry data in Figure 2b is consistent with the electrochemical data in Figure 1 and points to a conversion of $[(Cor)]H_3$ to $[(Cor)H_2]^-$ in PhCN only after the controlled-potential electroreduction of **9** at −1.20 V. The electrogenerated $[(Cor)H_2]^-$ is further reduced in PhCN at $E_{1/2} = -1.60$ and −1.90 V, and these potentials can be compared to quite similar $E_{1/2}$ values of −1.52 and −1.86 V for $[(Cor)H_2]^-$ reduction in pyridine, the small differences being due to differences in liquid-junction potentials and solvation differences between the two solvents.

Additional proof for the assignment of $[(Cor)H_2]^-$ as the $(Cor)H_3$ reduction product in PhCN comes from the fact that the new oxidation/reduction couple seen on the reverse scan in PhCN has a half-wave potential ($E_{1/2} = 0.21$ V) that closely matches that for the first oxidation of $[(Cor)H_2]^-$ at $E_{1/2} = 0.27$ V in pyridine. Because there is no evidence for the direct reduction of free H^+ in PhCN (which occurs at $E_p = -0.44$ V for a 10^{-3} M solution of $HClO_4$, Figure 1b), $(Cor)H_3$ is assigned as the electroactive species that initially accepts an electron to give $[(^{\bullet}Cor)H_3]^-$ at $E_p = -1.03$ V in this solvent. The electrogenerated $[(^{\bullet}Cor)H_3]^-$ is then converted to $[(Cor)H_2]^-$ as shown in eq 2a

$$(Cor)H_3 \overset{e}{\rightleftharpoons} [(^{\bullet}Cor)H_3]^- \rightarrow [(Cor)H_2]^- + \frac{1}{2}H_2 \qquad (2a)$$

but the time scale of this chemical reaction, which follows electron transfer, is sufficiently slow so as to allow a further reduction of any remaining $[(^{\bullet}Cor)H_3]^-$ on the electrode surface. This electrode reaction at the conjugated corrole macrocycle is proposed to occur for **9** at $E_p = -1.40$ V (Figure 1a). The concentration of $[(^{\bullet}Cor)H_3]^-$ **9** in PhCN and hence the peak current for the process at −1.40 V are substantially reduced because of the formation of $[(Cor)H_2]^-$, and a similar irreversible process with reduced current height is seen for 6 of the other 10 compounds through routine cyclic voltammetry under the same solution conditions. The peak potential for this reduction ranges from −1.40 to −1.56 V, and these values are summarized in Table 1.

Spectroscopic Characterization of $[(Cor)H_2]^-$, $(^{\bullet}Cor)H_2$, and $[(^{\bullet}Cor)H_2]^{2-}$. Thin-layer spectroelectrochemistry was used to electrogenerate in situ and spectroscopically characterize pure samples of $[(Cor)H_2]^-$, $(^{\bullet}Cor)H_2$, and $[(^{\bullet}Cor)H_2]^{2-}$. The relevant electrode reactions giving $[(Cor)H_2]^-$ are shown in eqs 2a (PhCN) and 2b (py), and examples of the thin-layer spectral changes obtained during the controlled-potential reduction are shown in Figure 3 for the case of compound $[(CNPh)_3Cor]H_3$ (**7**), where the reduction was carried out in PhCN (Figure 3a) or pyridine (Figure 3b).

$$(Cor)H_3 + py \rightleftharpoons [(Cor)H_2]^- + pyH^+ \qquad (2b)$$
$$\downarrow e$$
$$\tfrac{1}{2}H_2 + py$$

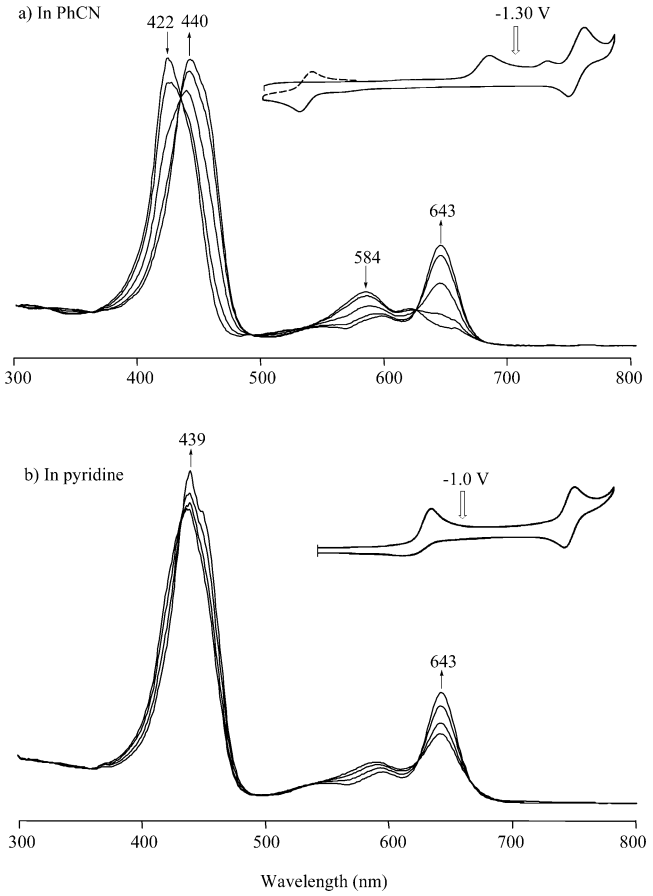

Figure 3. UV−visible spectral changes obtained during the thin-layer controlled-potential electroreduction of $[(CNPh)_3Cor]H_3$ (**7**) at (a) −1.30 in PhCN and (b) −1.00 V in pyridine, 0.1 M TBAP.

The electroactive form of the corrole in PhCN is undissociated $(Cor)H_3$ that, in the case of $[(CNPh)_3Cor]H_3$ (**7**), is characterized by a Soret band at 422 nm, a shoulder at 443 nm, and two visible bands at 584 and 619 nm. Controlled-potential reduction at −1.30 V in a thin-layer cell leads to the quantitative formation of $[(Cor)H_2]^-$ that, in the case of compound **7**, is characterized by a Soret band at 440 nm, a shoulder at 452 nm, and three visible bands at 546, 595, and 643 nm, the latter of which has a relatively high molar absorptivity.

As mentioned earlier, and shown in Table 2, one of two different UV−visible spectral patterns is observed for $(Cor)H_3$ in PhCN prior to the first reduction. One group of compounds has a split Soret band with a maximum intensity at 421−424 and 437−443 nm and a ratio of molar absorptivities between the two peaks of 1.3 and 1.5. The other group, with one exception (compound **10**), has a split Soret band at 412−416 and 425−432 nm and a ratio between the split Soret band intensities of 1.1 and 1.2. Other spectral differences are also observed between the corroles in the two series that are labeled group A and group B in Charts 1 and 2. The compounds in group B can be considered to be sterically hindered corroles on the basis of similar assignments in the case of substitutent tetraphenyl porphyrins.[21]

Despite differences in the UV−visible spectra of the neutral compound, similar types of spectral changes are seen during the first reduction in PhCN, and the UV−visible data

Table 2. UV−Visible Spectral Data, λ (nm, $\epsilon \times 10^{-4}$ M^{-1} cm^{-1}), of $(Cor)H_3$ and $[(Cor)H_2]^-$ in PhCN Containing 0.1 M TBAP

		$(Cor)H_3$					$[(Cor)H_2]^-$				
		Soret region			visible region		Soret region		visible region		
group type	compd	I	II	ϵ_I/ϵ_{II}							
A	**1**	421 (10.6)	437 (7.9)	1.3	584 (1.5)	622 (1.4)	430 (12.5)	452 (9.0)	536 (0.7)	596 (1.1)	644 (4.4)
	4	422 (9.4)	443 (6.3)[a]	1.5	584 (1.7)	620 (1.2)	439 (10.7)	452 (9.3)[a]	545 (0.7)	596 (1.0)	645 (3.6)
	7	422 (11.7)	443 (7.8)[a]	1.5	584 (2.1)	619 (1.5)	440 (11.6)	452 (10.3)[a]	546 (0.7)	595 (1.2)	643 (4.0)
	8	421 (8.3)	437 (6.1)[a]	1.4	581 (1.6)	612 (1.0)	440 (9.7)		554 (0.5)	595 (0.9)	640 (2.7)
	9	424 (11.3)	442 (8.3)[a]	1.4	585 (2.2)	620 (1.5)	445 (12.4)		558 (0.9)	597 (1.3)	643 (3.9)
B	**2**	414 (11.8)	432 (10.2)	1.2	571 (1.9)	605 (1.1)	432 (10.2)	464 (7.7)	553 (1.3)	587 (1.5)	633 (5.5)
	3	412 (7.5)	430 (6.3)	1.2	570 (1.3)	604 (0.9)	430 (7.3)	451 (7.5)	549 (0.5)	584 (0.7)	631 (2.8)
	5	414 (10.0)	430 (8.5)	1.2	571 (1.8)	609 (1.1)	432 (10.6)	449 (11.1)	550 (0.7)	590 (1.1)	630 (3.5)
	6	416 (14.0)	432 (12.5)	1.1	571 (2.7)	609 (1.6)	435 (12.5)	449 (12.0)	553 (1.2)	589 (1.5)	631(5.3)
	10	421 (13.5)			570 (2.7)	607 (1.6)	442 (14.9)		547 (1.0)	589 (1.4)	623 (3.2)
	11	413 (12.6)	425 (11.0)[a]	1.1	566 (2.2)	605 (1.3)	437 (16.8)		547 (0.7)	587 (1.4)	618 (3.3)

[a] Shoulder peak.

Table 3. UV−Visible Spectral Data, λ (nm, $\epsilon \times 10^{-4}$ M^{-1} cm^{-1}), of Electrogenerated $[(Cor)H_2]^-$ and $(^{\bullet}Cor)H_2$ in Pyridine or PhCN Containing 0.1 M TBAP

		$[(Cor)H_2]^-$ in py		$[(Cor)H_2]^-$ in py			$(^{\bullet}Cor)H_2$ in py		$(^{\bullet}Cor)H_2$ in PhCN	
		Soret region		visible region			Soret region		Soret region	
group type	compd									
A	**1**	427 (12.0)	450 (8.2)	540 (0.7)	595 (1.1)	643 (3.8)	393 (5.6)	433 (6.5)	396 (3.8)[a]	436 (4.8)
	4	438 (11.8)	452 (10.0)[a]	546 (0.7)	596 (1.1)	645 (3.7)		418 (9.2)		420 (8.5)
	7	439 (11.0)	449 (9.7)[a]	549 (0.5)	595 (0.9)	643 (3.3)		418 (8.8)		420 (10.6)
	8	437 (10.7)		556 (0.4)	595 (0.8)	639 (3.1)		415 (7.5)		417 (7.6)
	9	443 (13.4)		555 (0.8)	595 (1.2)	643 (3.9)		416 (11.1)		417 (10.3)
B	**2**	430 (9.5)	460 (6.8)	553 (1.0)	586 (1.2)	633 (4.9)	396 (9.8)	412 (9.5)	396 (9.7)	413 (9.6)
	3	428 (12.8)	449 (11.7)	549 (1.0)	587 (1.2)	631 (5.1)	398 (10.6)[a]	408 (11.6)	397 (5.4)[a]	410 (6.1)
	5	431 (11.3)	447 (10.7)	551 (0.6)	590 (1.0)	629 (3.6)	398 (7.6)[a]	413 (10.1)	399 (7.3)[a]	413 (9.0)
	6	434 (10.6)	449 (10.3)	553 (0.9)	589 (1.1)	630 (4.6)		415 (10.4)		417 (12.8)
	10	438 (12.6)		548 (1.4)	587 (1.6)	622 (3.2)		408 (8.7)		408 (9.1)
	11	435 (13.5)		547 (0.7)	587 (1.5)	617 (3.0)		411 (8.3)		413 (11.3)

[a] Shoulder peak.

in this solvent are summarized in Table 2, which gives the values of λ_{max} and ϵ for the two pure forms of free-base corroles in PhCN, that is, $(Cor)H_3$ before reduction and $[(Cor)H_2]^-$ after reduction.

The extent of H^+ dissociation from $(Cor)H_3$ is close to 100% for compounds **9** and **11** in pyridine, giving $[(Cor)H_2]^-$ prior to electroreduction, but incomplete dissociation occurs for the other nine investigated corroles, as determined by measuring the intensity of the most intense Q band for $[(Cor)H_2]^-$ before and after carrying out the first electroreduction.[28] An example of this is shown in Figure 3b for compound **7** in pyridine. The 643 nm band assigned to $[(Cor)H_2]^-$ increases in intensity by about 40% after reduction at −1.0 V, and this is consistent with a solution that initially contains 40% $(Cor)H_3$ and 60% $[(Cor)H_2]^-$. However, the reduction of pyH^+ at −1.0 V leads to a shift of the equilibrium in eq 2b such that all of the remaining $(Cor)H_3$ corrole is converted to its $[(Cor)H_2]^-$ form, and the final spectrum in pyridine (Figure 3b) is virtually identical to the final spectrum of the electroreduced product in PhCN (Figure 3a). This spectrum of $[(Cor)H_2]^-$ (**7**) in pyridine is characterized by a Soret band at 439 nm, a shoulder at 449 nm, and three visible bands at 549, 595, and 643 nm. These spectral data and those of the other 10 electrogenerated $[(Cor)H_2]^-$ derivatives in pyridine are given in Table 3 after complete reduction of the liberated proton (pyH^+) in a thin-layer cell and are virtually identical to the data for the same electrogenerated compounds in PhCN (Table 2). Again, two distinct types of spectral patterns are observed. Group A compounds in pyridine all have an intense Q band at 639−645 nm, whereas the group B derivatives in the same solvent show an intense Q band at 617−633 nm.

The UV−visible spectra of each neutral $(^{\bullet}Cor)H_2$ radical in pyridine and PhCN were obtained after thin-layer electrooxidation of $[(Cor)H_2]^-$, and a summary of the spectral data for this form of the free-base corrole in the two solvents is given in Table 3. The spectra in PhCN were taken after the oxidation of electrogenerated $[(Cor)H_2]^-$; however, in pyridine a direct controlled-potential oxidation at 0.40 V leads to $(^{\bullet}Cor)H_2$ in a thin-layer cell.

An example of the thin-layer spectral changes obtained during the first controlled-potential oxidation in pyridine is shown in Figure 4a,where the electrode reaction occurs as shown in eq 3. The final product of oxidation is a neutral corrole radical, and this was verified by measuring the ESR spectrum for compound **2**, which showed a strong organic radical signal at $g = 2.0047$.

$$(Cor)H_3 \overset{-H^+}{\rightleftharpoons} [(Cor)H_2]^- \rightleftharpoons (^{\bullet}Cor)H_2 + e \qquad (3)$$

Although less than 100% of $[(Cor)H_2]^-$ may be present in pyridine,[28] as the oxidation of $[(Cor)H_2]^-$ to $(^{\bullet}Cor)H_2$

(28) The percentage of initial $[(Cor)H_2]^-$ in pyridine ranges from 13 to 100% and was calculated using data of the type shown in Figure 3b. The results are as follows: **1** (19%), **2** (16%), **3** (13%), **4** (60%), **5** (52%), **6** (47%), **7** (58%), **8** (74%), **9** (95%), **10** (45%), and **11** (100%).

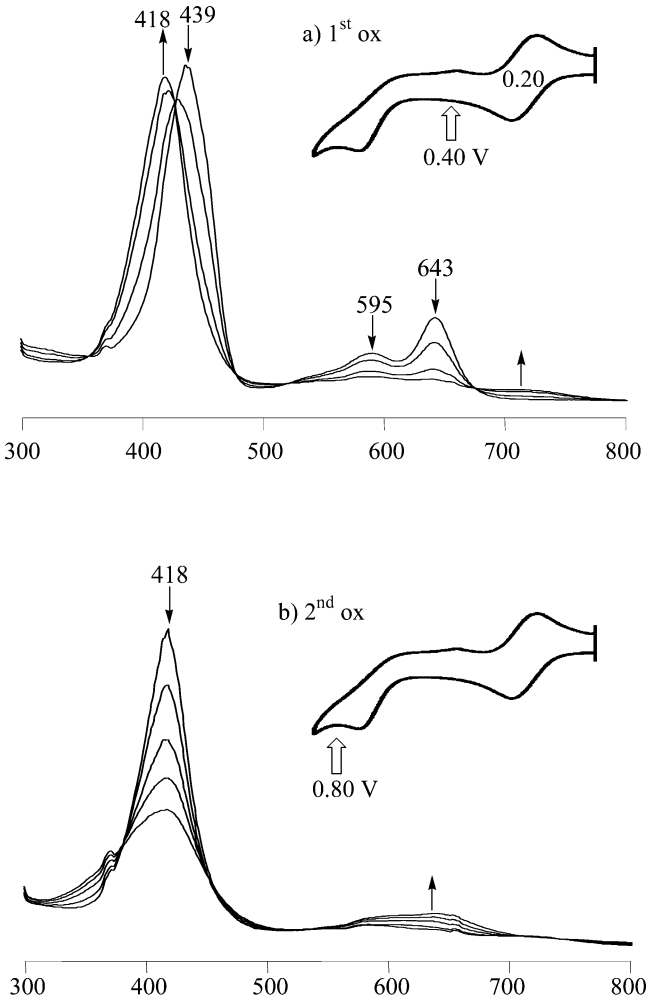

Figure 4. UV−visible spectral changes during the thin-layer controlled-potential electrooxidation of $[(CNPh)_3Cor]H_3$ (**7**) in pyridine, 0.1 M TBAP at (a) 0.40 V and (b) 0.80 V.

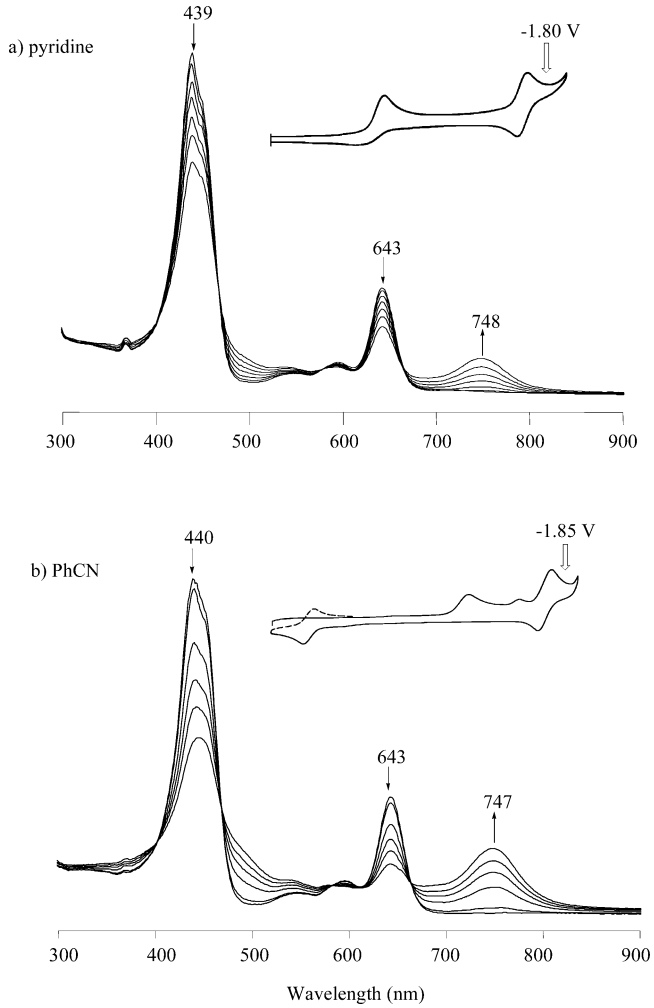

Figure 5. UV−visible spectral changes during the thin-layer controlled-potential electroreduction of $[(CNPh)_3Cor]H_3$ (**7**) at (a) −1.80 V in pyridine and (b) −1.85 V in PhCN, 0.1 M TBAP.

proceeds, the equilibrium in eq 3 is shifted to the right, and all of the $(Cor)H_3$ is consumed. As seen in Table 3, the final spectra of the $(^{\bullet}Cor)H_2$ derivatives in pyridine are virtually the same as those in PhCN.

Finally, the irreversible oxidation of $(^{\bullet}Cor)H_2$ in pyridine (at E_p = 0.54 to 0.84 V) and the reversible reduction of $[(Cor)H_2]^-$ in the same solvent (at $E_{1/2}$ = −1.57 to −1.85 V) were investigated by thin-layer spectroelectrochemistry for selected compounds. Examples of the UV−visible spectral changes obtained during these two processes are shown in Figures 4b (oxidation) and 5a (reduction) for compound **7** in pyridine. Thin-layer electroreduction of **7** was also investigated in PhCN, and the spectroelectrochemical data is shown in Figure 5b. Both sets of spectral changes during the reduction of $[(Cor)H_2]^-$ (Figure 5a and b) are consistent with the formation of a corrole π-anion radical, $[(^{\bullet}Cor)H_2]^{2-}$, in that there is a reduced-intensity Soret band and a broad visible band at 747−748 nm. The relevant electrode reaction that results in this species is shown in eq 4

$$[(Cor)H_2]^- + e \rightleftharpoons [(^{\bullet}Cor)H_2]^{2-} \qquad (4)$$

Electrooxidation of $(Cor)H_3$ in PhCN. The electrooxidation of $(Cor)H_3$ at a Pt electrode in PhCN consists of four redox couples, as shown in Figure 6 for compound **9**. The first oxidation of **9** (labeled rxn I) is irreversible and is located at E_p = 0.72 V for a scan rate of 0.1 V/s. The process is coupled to a rereduction peak at E_p = 0.26 V on the return negative potential sweep (rxn II).

Similar current−voltage curves were obtained for all of the investigated free-base corroles in PhCN (selected examples in Figure 7) although three of the compounds (**3**, **5**, and **8**) showed complicated behavior due to the involvement of pyridyl substituents in acid−base reactions. The voltammograms in Figures 6 and 7 show no apparent mechanistic differences in the oxidation behavior between the nonsterically hindered corroles in the group A series (**9** and **4**) and the sterically hindered derivatives in the group B series (**2**, **6**, and **10**). The anodic peak potential for the first oxidation of $(Cor)H_3$ ranged from E_p = 0.38 to 0.86 V at a scan rate of 0.1 V/s, whereas the coupled rereduction peak was located between E_{pc} = 0.00 and 0.42 V, with $E_{pa} - E_{pc}$ values being separated by 250−530 mV. The exact peak potentials are listed in Table 4 where rxns II−V are assigned as electrode reactions of species generated in the initial

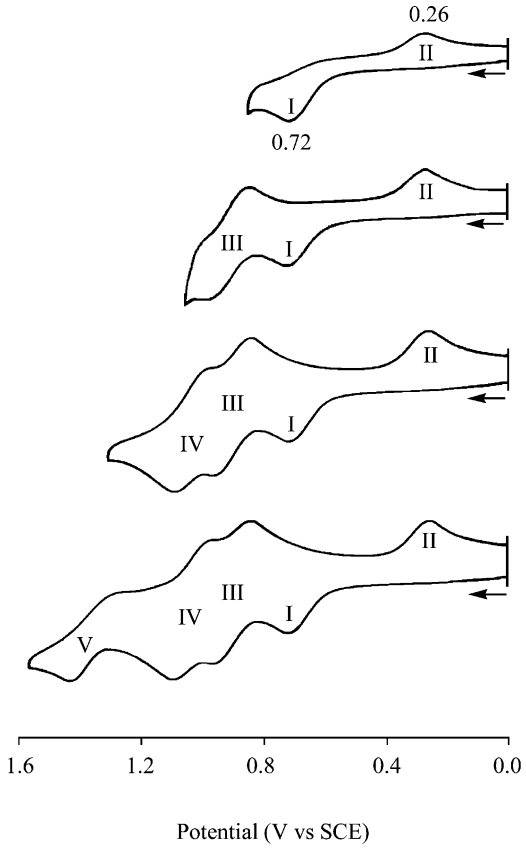

Figure 6. Cyclic voltammograms illustrating the oxidation of $[((CF_3)_2Ph)_3Cor]H_3$ (**9**) in PhCN, 0.1 M TBAP at a Pt electrode.

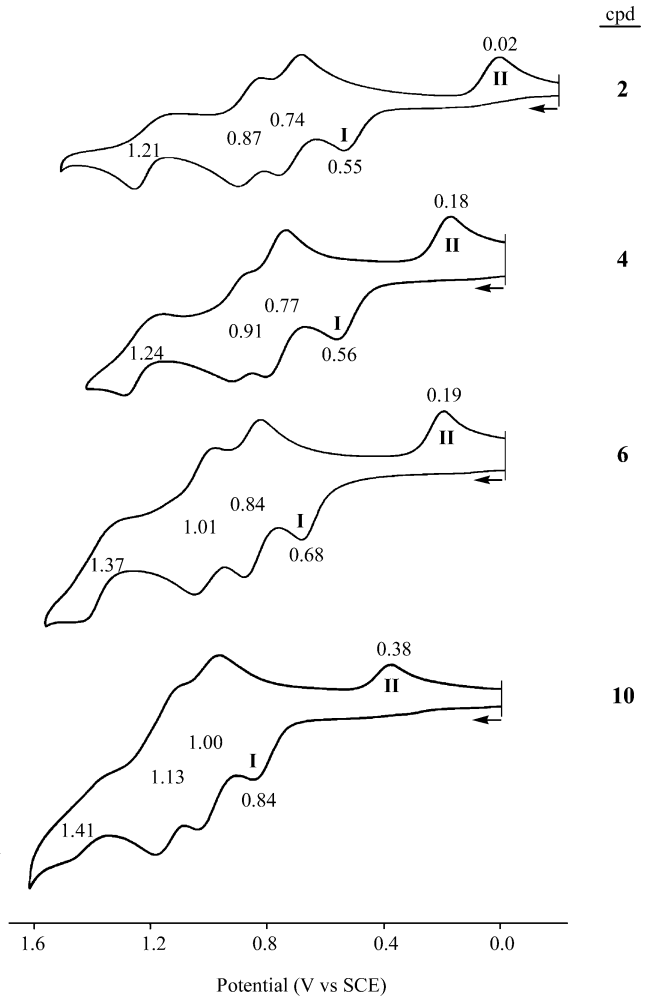

Figure 7. Cyclic voltammograms illustrating the oxidation of $[(Me_3Ph)_2(CNPh)Cor]H_3$ (**2**), $[(CF_3Ph)_3Cor]H_3$ (**4**), $[(Cl_2Ph)_2(CNPh)Cor]H_3$ (**6**), and $[(F_4N_3Ph)_3Cor]H_3$ (**10**) in PhCN, 0.1 M TBAP. Scan rate: 0.1 V/s.

electrooxidation (rxn I). Some of the processes are associated with $(^{\bullet}Cor)H_2$, and the others can be assigned as associated with $[(Cor)H_4]^+$, as indicated in the following discussion.

Earlier electrochemical studies on the oxidation of $(OEC)H_3$ by linear-sweep voltammetry in CH_2Cl_2 showed the presence of four processes,[18] the latter two of which were assigned to an electron abstraction from $[(OEC)H_4]^+$ generated as a product of the first oxidation in solution. The formation of $[(Cor)H_4]^+$ was also detected as an oxidation product of the currently investigated free-base corroles in PhCN, but this was accompanied by significant concentrations of $(^{\bullet}Cor)H_2$.

Evidence of mixtures of $(^{\bullet}Cor)H_2$ and $[(Cor)H_4]^+$ as products of the first oxidation (rxn I) is given in part by the presence of rxn II, assigned to the $(^{\bullet}Cor)H_2$ reduction, and by a comparison of UV−visible spectroelectrochemistry data obtained during rxn I with spectra of pure $(^{\bullet}Cor)H_2$ and $[(Cor)H_4]^+$ samples in the absence of a mixture. The UV−visible spectra of $(^{\bullet}Cor)H_2$ are summarized for each compound in Table 3. The spectra of $[(Cor)H_4]^+$ were not available prior to this study and were therefore measured in PhCN after the in situ generation from $(Cor)H_3$ solutions to which trifluroacetic acid (TFA) in sufficient quantity had been added to produce the protonated free-base corroles. In all cases, the addition of one H^+ from TFA to $(Cor)H_3$ proceeds stoichiometrically, indicating the complete conversion to $[(Cor)H_4]^+$. The protonated corroles are characterized by a well-defined visible band between 632 and 694 nm,

Table 4. Half-Wave Potentials (V vs SCE) for the Oxidation of $(Cor)H_3$ and the Reaction of Its Oxidation/Reduction Products at a Pt Electrode in PhCN Containing 0.1 M TBAP

	reactant	products			
	$(Cor)H_3$	$(^{\bullet}Cor)H_2$		$[(Cor)H_4]^+$	*c*
initial compd	I[a]	II[a]	IV	III	V
$[(MePh)_3Cor]H_3$ (**1**)	0.38	0.00	0.68	0.60	1.03
$[(Me_3Ph)_2(CNPh)Cor]H_3$ (**2**)	0.55	0.02	0.87	0.74	1.21
$[(Me_3Ph)_2(py)Cor]H_3$ (**3**)[b]					
$[(CF_3Ph)_3Cor]H_3$ (**4**)	0.56	0.18	0.91	0.77	1.24
$[(Cl_2Ph)_2(py)Cor]H_3$ (**5**)[b]					
$[(Cl_2Ph)_2(CNPh)Cor]H_3$ (**6**)	0.68	0.19	1.01	0.84	1.37
$[(CNPh)_3Cor]H_3$ (**7**)	0.58	0.20	0.91	0.79	1.24
$[(py)_2(F_2Ph)Cor]H_3$ (**8**)[b]					
$[((CF_3)_2Ph)_3Cor]H_3$ (**9**)	0.70	0.29	1.01	0.89	1.39
$[(F_4N_3Ph)_3Cor]H_3$ (**10**)	0.84	0.38	1.13	1.00	1.41
$[(F_5-Ph)_3Cor]H_3$ (**11**)	0.86	0.42	1.16	1.04	1.45

[a] Peak potential at a scan rate of 0.1 V/s. [b] Ill-defined peaks did not allow the assignment of potentials or processes. [c] Unassigned reaction.

and a similar intense band is not seen for either $(Cor)H_3$ or $(^{\bullet}Cor)H_2$ (Tables 2 and 3). The complete UV−visible spectral data for each protonated free-base corrole in PhCN are summarized in Table 5 and arranged in the same two groups as those for $(Cor)H_3$ and $[(Cor)H_2]^-$. Here the main differ-

Table 5. UV−Visible Spectral Data, λ (nm, $\epsilon \times 10^{-4}$ M^{-1} cm^{-1}), of $[(Cor)H_4]^+$ in PhCN

group type	compd[a]	Soret bands		visible bands		
A	$[(MePh)_3Cor]H_3$ (**1**)	428 (8.8)	459 (5.7)	544 (0.6)		694 (3.2)
	$[(CF_3Ph)_3Cor]H_3$ (**4**)	429 (9.4)	454 (5.9)[b]	549 (0.5)		679 (2.6)
	$[(CNPh)_3Cor]H_3$ (**7**)	428 (11.8)	452 (7.3)[b]	548 (0.7)		677 (2.9)
	$[((CF_3)_2Ph)_3Cor]H_3$ (**9**)	429 (12.0)	449 (7.7)[b]	547 (0.6)		671 (2.8)
B	$[(Me_3Ph)_2(CNPh)Cor]H_3$ (**2**)	422 (11.6)	444 (10.4)	537 (0.8)		652 (2.7)
	$[(Me_3Ph)_2(py)Cor]H_3$ (**3**)		466 (6.1)	557 (0.5)	610 (0.8)	651 (1.2)
	$[(Cl_2Ph)_2(py)Cor]H_3$ (**5**)		459 (9.3)	557 (0.8)	599 (1.0)	646 (1.8)
	$[(Cl_2Ph)_2(CNPh)Cor]H_3$ (**6**)	423 (14.4)	444 (12.3)	560 (1.0)	598 (1.3)	647 (3.1)
	$[(F_4N_3Ph)_3Cor]H_3$ (**10**)	426 (14.6)		550 (0.7)	593 (0.9)	639 (2.2)
	$[(F_5-Ph)_3Cor]H_3$ (**11**)	420 (13.2)		548 (0.5)	588 (0.8)	632 (1.7)

[a] Compound **8** is not included because it contains two pyridyl groups that react with acid and limit the measurement. [b] Shoulder peak.

ence between the spectral patterns in groups A and B is in the position of the Q band. The protonated corroles in the group A series have the most intense Q bands located at 671−694 nm, whereas the compounds in the group B series have strong Q bands at 632−652 nm.

The combined electrochemical and spectroelectrochemical data of compounds **1**−**11** suggests that the oxidation of $(Cor)H_3$ in PhCN first produces $[(^{\bullet}Cor)H_3]^+$, which is a strong acid and rapidly loses a proton, giving $(^{\bullet}Cor)H_2$ and H^+. The liberated H^+ then reacts with another molecule of neutral $(Cor)H_3$ to produce $[(Cor)H_4]^+$ and thus gives a mixture of $(^{\bullet}Cor)H_2$ and $[(Cor)H_4]^+$ oxidation products, as shown in eqs 5a and 5b:

$$(Cor)H_3 \overset{-e}{\rightleftharpoons} [(^{\bullet}Cor)H_3]^+ \rightarrow (^{\bullet}Cor)H_2 + H^+ \qquad (5a)$$

$$(Cor)H_3 + H^+ \rightleftharpoons [(Cor)H_4]^+ \qquad (5b)$$

The relative concentrations of $(^{\bullet}Cor)H_2$ and $[(Cor)H_4]^+$ generated as products of rxn I in PhCN will depend on the basicity of the neutral $(Cor)H_3$, which in turn will depend on the specific electron-donating or electron-withdrawing substituents on the three meso positions of the macrocycle. We expected to obtain a larger concentration of $[(Cor)H_4]^+$ for the investigated corroles with meso-substituted electron-donating groups than for those with electron-withdrawing substituents, and this is what we observed by comparing the spectra obtained during the first oxidation of $[(Me_3Ph)_2(CNPh)Cor]H_3$ (**2**) and $[((CF_3)_2Ph)_3Cor]H_3$ (**9**) with the UV−visible spectra for the fully protonated corroles $[((Me_3Ph)_2(CNPh)Cor)H_4]^+$ and $[(((CF_3)_2Ph)_3Cor)H_4]^+$ obtained by titration with TFA in PhCN solutions. Compound **9** has three electron-withdrawing $(CF_3)Ph$ substituents, and compound **2** has two strong electron-donating Me_3Ph substituents, thus giving two extremes of free-base corrole basicity.

A comparison between the UV−visible spectra of electro-oxidized $(Cor)H_3$ and $[(Cor)H_4]^+$ generated by titration with TFA is given in Figure 8. A well-defined 652 nm band is observed during the first oxidation of compound **2** (Figure 8a), and the same 652 nm band is seen for $[((Me_3Ph)_2(CNPh)Cor)H_4]^+$ generated upon titration of $[(Me_3Ph)_2(CNPh)Cor]H_3$ (**2**) with TFA in PhCN (Figure 8b). In contrast, $[(((CF_3)_2Ph)_3Cor)H_4]^+$ (**9**) has a strong 671 nm band in PhCN (Figure 8d), but this band is missing in the spectrum obtained after electrooxidation of $[((CF_3)_2Ph)_3Cor]H_3$ (**9**) in PhCN (Figure 8c). This result clearly indicates the presence of a larger amount of the $[(Cor)H_4]^+$ product after the one-electron oxidation of compound **2** than after the same electrooxidation of compound **9**.

The most compelling evidence suggesting $(^{\bullet}Cor)H_2$ as a second corrole oxidation product in rxn I is the appearance of rxn II, which is not present in PhCN until after the electrooxidation of $(Cor)H_3$. The cathodic peak potentials for rxn II are similar to the values of $E_{1/2}$ for the $(^{\bullet}Cor)H_2/[(Cor)H_2]^-$ couple of the electrogenerated species produced in the same solvent during the electroreduction of $(Cor)H_3$ (Table 1 and Figure 1). This similarity in potentials strongly suggests the formation of $(^{\bullet}Cor)H_2$ upon the electrooxidation of $(Cor)H_3$ in PhCN (rxn I) and then its rereduction via rxn II to give $[(Cor)H_2]^-$ upon reversing the potential-sweep direction.

The initial oxidation of $(Cor)H_3$ in rxn I and the proposed reduction of the $(^{\bullet}Cor)H_2$ product in rxn II both involve a chemical reaction following electron transfer (an electrochemical (EC) mechanism), and the classic box mechanism given in Scheme 2 is proposed, where reactions Ia and Ib combined represent the EC mechanism for the oxidation in rxn I and reactions IIa and IIb combined are those associated with the reduction in rxn II (Figure 6). The liberated proton in the first oxidation step reacts with a second $(Cor)H_3$ molecule to give $[(Cor)H_4]^+$, as shown in eq 5b.

Additional evidence for the formation of both $(^{\bullet}Cor)H_2$ and $[(Cor)H_4]^+$ as products of rxn I is given by the spectral data in Figure S2 (Supporting Information) for the electro-oxidation of compound **2** in a thin-layer cell. The first oxidation at 0.65 V produces a spectrum with Soret bands at 399, 420, and 444 nm and a Q band at 652 nm (Figure S2a). The spectrum of pure $(^{\bullet}Cor)H_2$ **2** in PhCN has a split Soret band at 396 and 413 nm (Table 3), whereas the spectrum of pure $[(Cor)H_4]^+$ **2** in the same solvent has a split Soret band at 422 and 444 nm and two visible bands at 537 (weak) and 652 nm (Table 5). The spectrum after the first oxidation is clearly a mixture of these two forms of the corrole, and classic equations for analyzing the UV−visible spectrum of a two-component mixture can be used to evaluate the relative concentrations of each using the

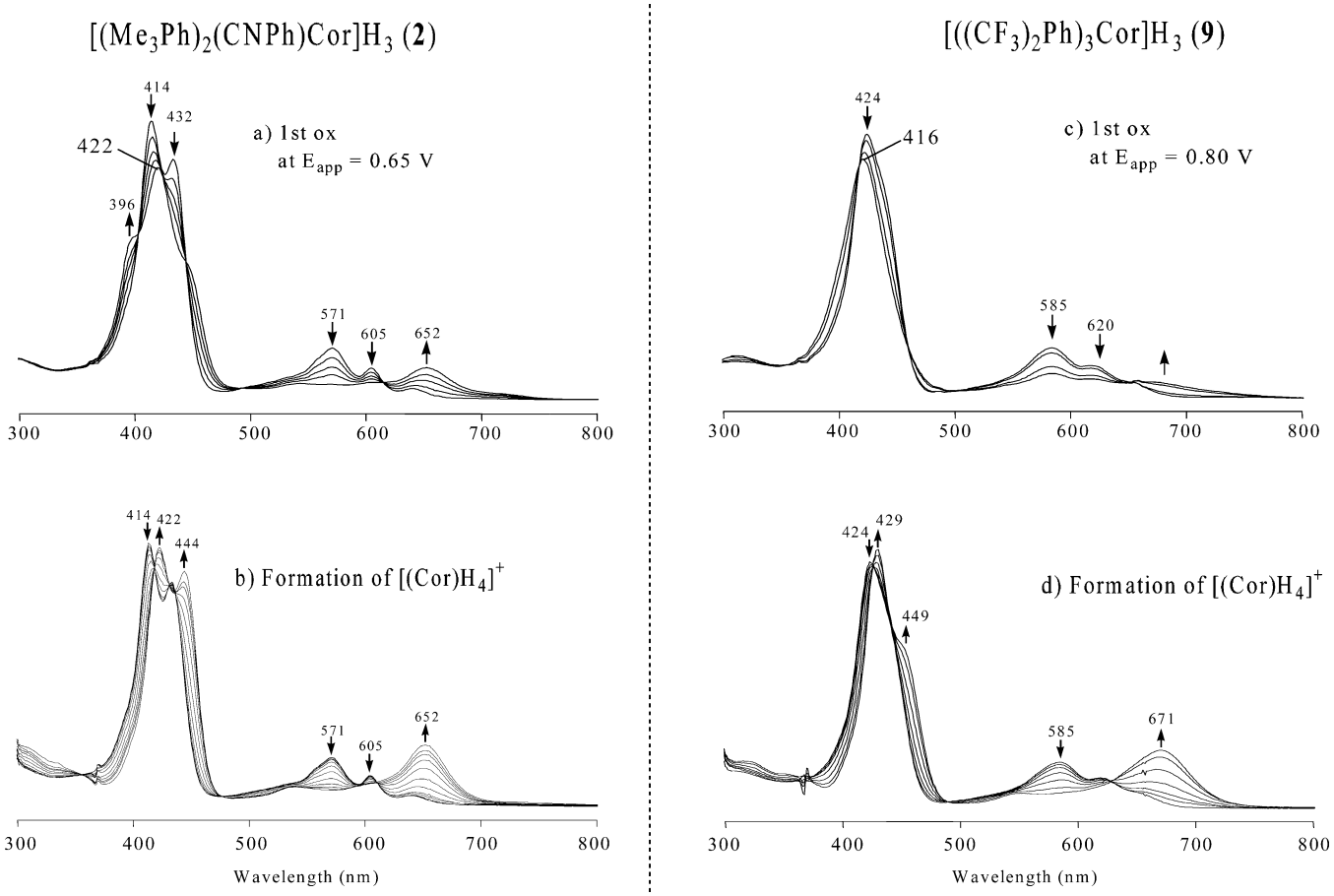

Figure 8. UV−visible spectral changes during the electrooxidation or titration of $[(Me_3Ph)_2(CNPh)Cor]H_3$ (**2**) and $[((CF_3)_2Ph)_3Cor]H_3$ (**9**) with TFA in PhCN.

Scheme 2

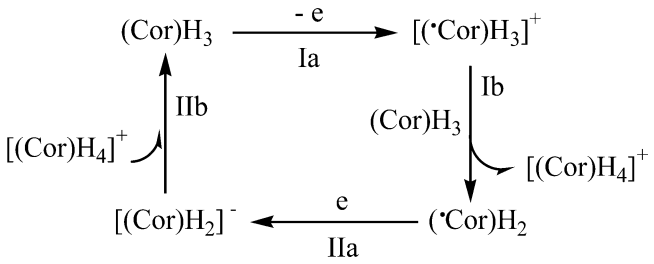

measured molar absorptivities of the pure compounds.[29] This analysis was carried out and gave a composite spectrum for a mixture containing 60% (•Cor)H_2 and 40% $[(Cor)H_4]^+$. This spectrum is shown in Figure S2. The maximum amount of $[(Cor)H_4]^+$ cannot exceed 50% in the absence of an added proton source, and thus the above analysis fits the sequence of steps given by eqs 5a and 5b.

Assignment of Other Oxidation Processes. Having determined that (•Cor)H_2 and $[(Cor)H_4]^+$ are the only corrole oxidation products in rxn I and that rxn II involves a conversion of (•Cor)H_2 to $[(Cor)H_2]^-$ facilitates the assignment of the additional oxidation processes observed in PhCN. The assignment then becomes even easier by monitoring the electrooxidation of $(Cor)H_3$ in PhCN solutions containing increasing amounts of TFA, thus maximizing the concentration of $[(Cor)H_4]^+$ in solution and decreasing to zero the concentration of any (•Cor)H_2 that would be electrogenerated in rxn I. This electrochemically monitored titration of $(Cor)H_3$ in PhCN containing TFA was also carried out at a glassy carbon electrode to monitor the electroreduction of $[(Cor)H_4]^+$ in the absence of overlapping currents due to the reduction of the added H^+. Although the reduction of the free proton in PhCN occurs at $E_p = -0.44$ V in PhCN at a Pt electrode (for 10^{-3} M $HClO_4$ solution), the same reaction is shifted to potentials more negative than −1.0 V when the reaction is carried out at a glassy carbon or Hg electrode as seen in Figure S1 (Supporting Information). This is in agreement with what has been reported in the literature.[26]

The results of an acid titration of $(Cor)H_3$ in PhCN are shown in Figure 9 for compound **2**, $[(Me_3Ph)_2(CNPh)Cor]H_3$, and are highly informative. As TFA is added to the solution and $[(Cor)H_4]^+$ is generated, the concentration of $(Cor)H_3$ decreases, as evidenced by a decreased current for rxn I. At the same time, the currents for rxns II and IV disappear as those for rxn III increase in magnitude to approximately double the initial value. At the same time, a new reduction peak appears at $E_{pc} = -0.62$ V, which reaches maximum intensity and then does not increase with further addition of TFA. This latter process is labeled as rxn VI. Only $[(Cor)H_4]^+$ is present in PhCN solutions containing 8.0 equiv of TFA; therefore, rxns II and IV that are no longer

(29) Skoog, D. A.; West, D. M.; Holler, F. J.; Crouch, S. R. *Fundamentals of Analytical Chemistry*, 8th ed.; Thomson-Brooks: Belmont, CA, 2004.

Table 6. HOMO−LUMO Gap (V) of Free-Base Corroles in Pyridine and PhCN Containing 0.1 M TBAP

		$[(Cor)H_2]^{-1}$ in pyridine			$[(Cor)H_2]^{-1}$ in PhCN			$(Cor)H_3$ in PhCN		
group type	compd	$E_{1/2}^{ox}$	$E_{1/2}^{red}$	HOMO−LUMO gap (V)	$E_{1/2}^{ox}$	$E_{1/2}^{red}$	HOMO−LUMO gap (V)	E_p^{ox}	E_p^{red}	HOMO−LUMO gap (V)
A	**1**	0.10	−1.85	1.95	−0.08	−1.91	1.83	0.38	−1.36	1.74
	4	0.18	−1.67	1.85	0.09	−1.71	1.80	0.56	−1.13	1.69
	7	0.20	−1.65	1.85	0.11	−1.72	1.83	0.58	−1.13	1.71
	8	0.24	−1.62	1.86	0.14	−1.67	1.81	[c]	−0.98	
	9	0.27	−1.52	1.79	0.21	−1.60	1.81	0.70	−1.03	1.73
	av[d]			1.86 ± 0.06			1.82 ± 0.01			1.72 ± 0.02
B	**2**	0.13	−1.96	2.09	−0.02			0.55	−1.30	1.85
	3	0.14	−1.93	2.07	−0.02			0.48	−1.33	1.81
	5	0.22	−1.80	2.02	0.09	−1.86	1.95	0.50	−1.21	1.71
	6	0.21	−1.78	1.99	0.10	−1.85	1.95	0.68	−1.23	1.91
	10	0.34	−1.64[a]	1.98	0.30	−1.82[b]		0.84	−1.02	1.86
	11	0.37	−1.57	1.94	0.31	−1.64	1.95	0.86	−1.04	1.90
	av[d]			2.02 ± 0.06			1.95 ± 0.00			1.84 ± 0.07

[a] Peak potential at a scan rate of 0.1 V/s. [b] The process overlapped with the reduction of the azide group on the corrole. [c] Ill-defined oxidation. [d] Av = averaged value.

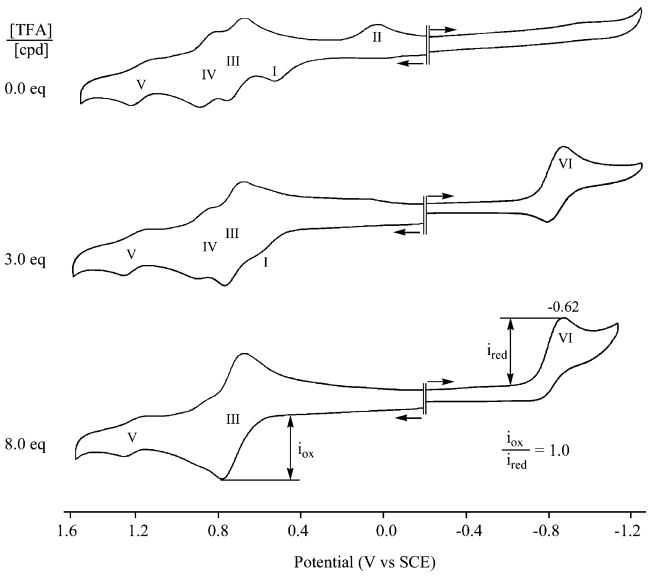

Figure 9. Cyclic voltammograms of 1.29×10^{-3} M $[(Me_3Ph)_2(CNPh)Cor]H_3$ (**2**) in PhCN, 0.1 M TBAP with different TFA concentrations.

present can be definitively assigned to the one-electron reduction and oxidation processes of $(^{\bullet}Cor)H_2$. The one-electron oxidation of $[(Cor)H_4]^+$ is assigned as rxn III, and the one-electron reduction of the same compound is assigned as rxn VI. Values of $E_{1/2}$ for these two processes are not very different from what was reported for the one-electron oxidation and reduction of $[(OEC)H_4]^+$ to its π-radical forms in CH_2Cl_2 (0.42 and −1.10 V vs Fc^+/Fc).[18]

The electrogenerated radical produced upon the reduction of $[(Cor)H_4]^+$ in PhCN is unstable in PhCN because of the loss or reduction of protons on the central nitrogens, but the electrooxidized $[(^{\bullet}Cor)H_4]^{2+}$ radical could be examined on the thin-layer spectroelectrochemical time scale and gave a species whose Soret and visible bands were significantly decreased in intensity, as would be expected when an electron is abstracted from the conjugated π-system of the macrocycle. These UV−vis spectra were not examined in detail except in the case of compound **9**, where $[(^{\bullet}Cor)H_4]^{2+}$ was measured for comparison with the other forms of the free-base corrole with the same macrocycle. The spectrum of $[(^{\bullet}Cor)H_4]^{2+}$ has a decreased-intensity Soret band at 432 nm

Scheme 3

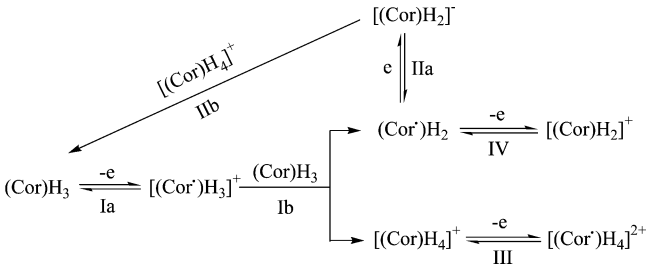

and a broad band in the visible region of the spectra between 550 and 850 nm, with a maximum at approximately 687 nm.

The above electrochemical results are self-consistent with the known acid/base properties of $(Cor)H_3$, and the overall oxidation/reduction mechanism of the 11 compounds in PhCN is given in Scheme 3, where the a and b parts of rxns I and II indicate the chemical steps following electron transfer in the forward and reverse steps.

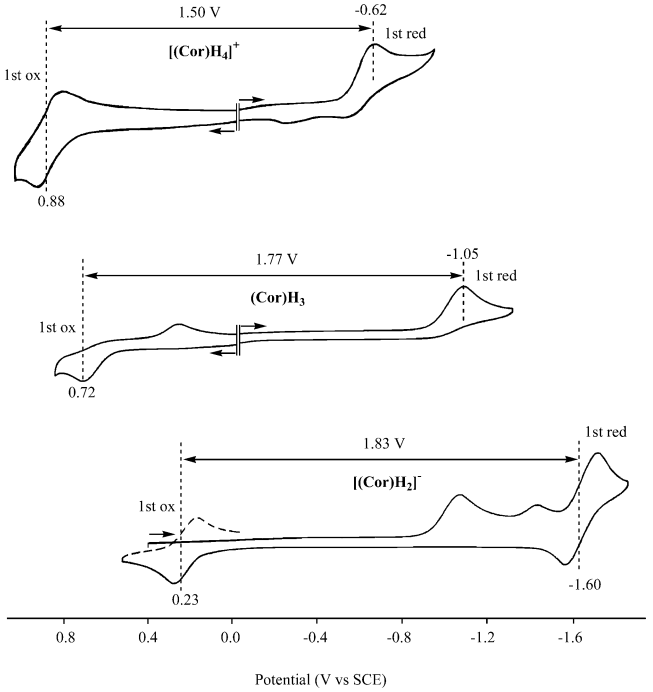

Figure 10. Illustration of the HOMO−LUMO gap (V) for different protonated forms of $[((CF_3)_2Ph)_3Cor]$ **9** in PhCN, 0.1 M TBAP.

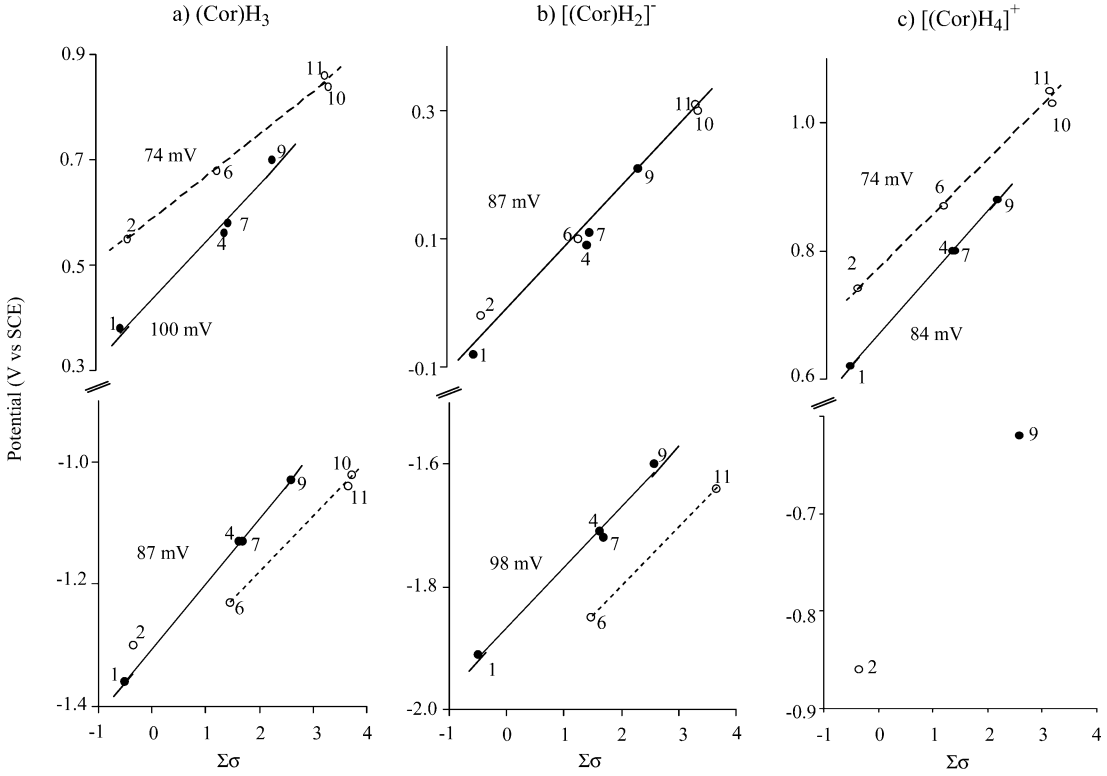

Figure 11. Plot of the potentials for the redox reactions of three free-base corrole species in PhCN, 0.1 M TBAP vs the sum of the Hammett constants ($\Sigma\sigma$) for the substituents on the three phenyl groups of the compounds. Hammett constants are taken from ref 32.

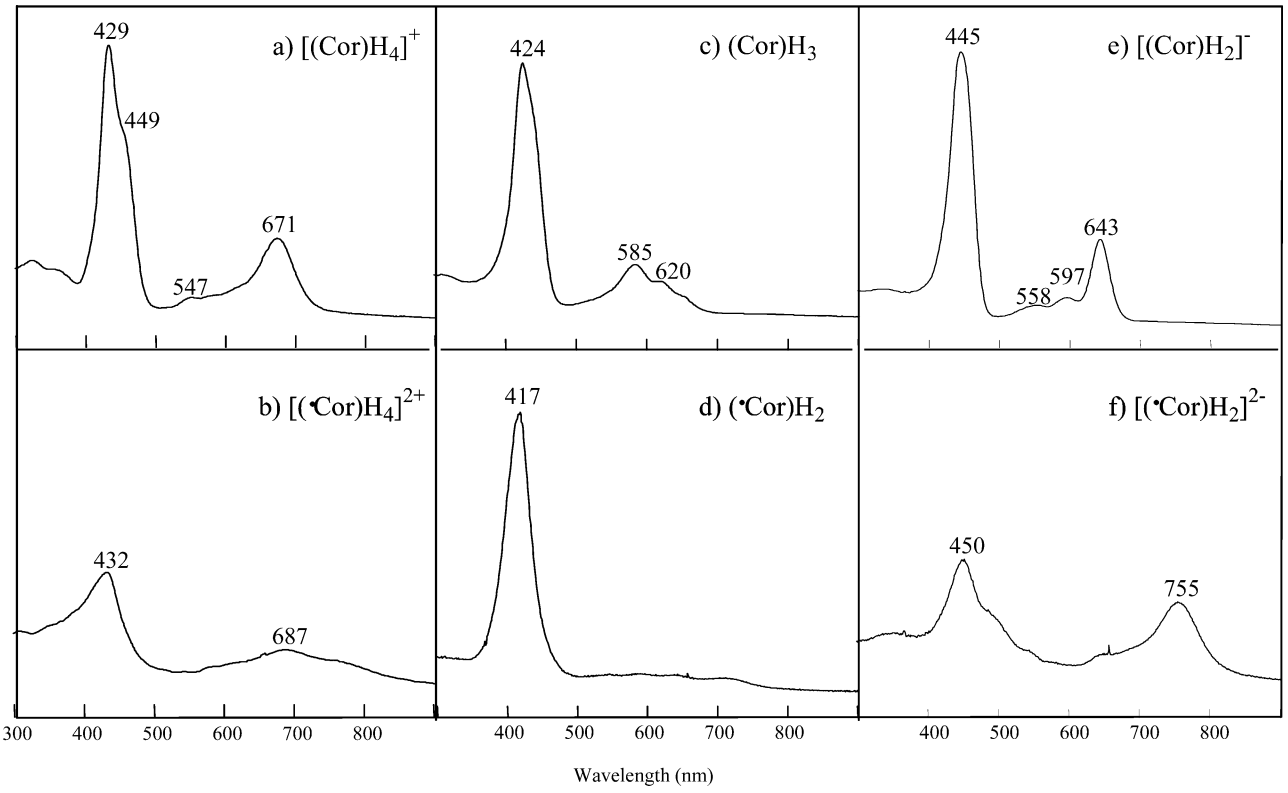

Figure 12. Comparative UV−visible spectra of different free-base corroles of [$((CF_3)_2Ph)_3$Cor] (**9**) in PhCN.

Because $[(Cor)H_4]^+$ is the only free-base corrole in PhCN solutions containing excess TFA, the reversible to quasi-reversible rxn V must be associated with this species, but its current height does not change with the increase in $[(Cor)H_4]^+$ concentration as might be expected. For this reason, an assignment of the oxidation reaction (rxn V) to a specific free-base corrole must be left to further studies.

Electrochemical HOMO−LUMO Gap and Linear Free-Energy Relationships. Because the neutral, protonated, and deprotonated forms of the free-base corrole can each be

Scheme 4

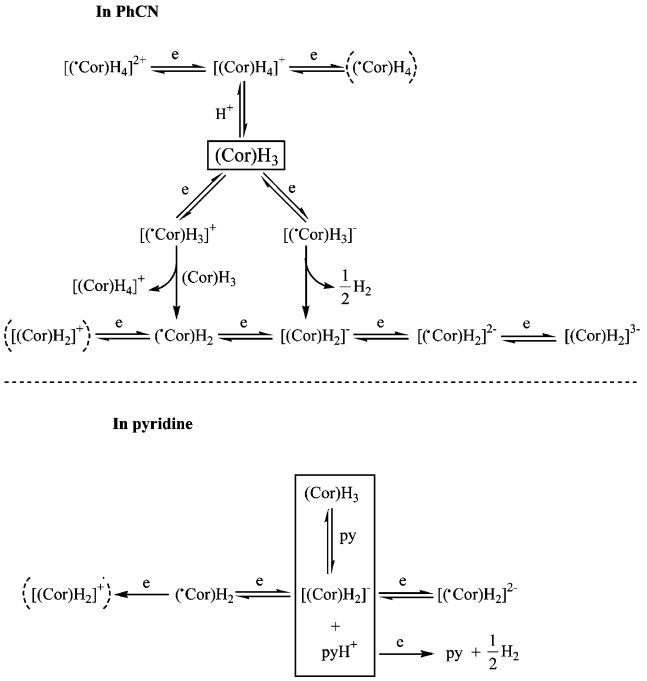

oxidized or reduced by one electron, measurements of the electrochemical HOMO−LUMO gaps for these three different species can be determined. The largest HOMO−LUMO gap is for $[(Cor)H_2]^-$, which averages 1.86 ± 0.06 and 2.02 ± 0.06 V for group A and group B compounds, respectively, in pyridine and 1.82 ± 0.01 and 1.95 V for the same two series of compounds in PhCN (Table 6). Slightly smaller HOMO−LUMO gaps of 1.72 ± 0.02 and 1.84 ± 0.07 V were determined for the two groups of $(Cor)H_3$ derivatives in PhCN, and a more significant decrease was observed for $[(Cor)H_4]^+$, whose oxidation and reduction potentials are separated by an average of 1.55 V for compounds **2** and **9** in PhCN, which is virtually the same value of $\Delta E_{1/2}$ reported in CH_2Cl_2 for $[(OEC)H_4]^+$ (1.52 V).[19] The individual HOMO−LUMO gap for each compound in the different solvents is summarized in Table 6, and a graphical comparison of the HOMO−LUMO gaps for the $[(Cor)H_4]^+$, $(Cor)H_3$, and $[(Cor)H_2]^-$ forms of compound **2** in PhCN is shown in Figure 10.

The differences in the HOMO−LUMO gap between sterically and nonsterically hindered corroles in groups A and B of $(Cor)H_3$ and $[(Cor)H_2]^-$ are associated with the differences in both HOMO and LUMO levels of the compounds, and this is shown in Figure 11, which plots the potentials for the first oxidation and the first reduction of $(Cor)H_3$, $[(Cor)H_2]^-$, and $[(Cor)H_4]^+$ versus the sum of the Hammett substituent constants on the meso-phenyl groups of the different complexes.[30] The nonsterically hindered corroles in the A group (**1**, **4**, **7**, and **9**) are represented by solid circles and the sterically hindered corroles in the B group (**2**, **6**, **10**, and **11**) are represented by open circles. The slope of the $\Delta E_{1/2}$ versus $\sum\sigma$ plot is defined by the reaction constant ρ,[31] which in the case of meso-substituted porphyrins[32] and meso-substituted corroles[14,15] generally ranges from 50 to 100 mV depending upon the solvent and the nature of the central metal ion, if one is present.

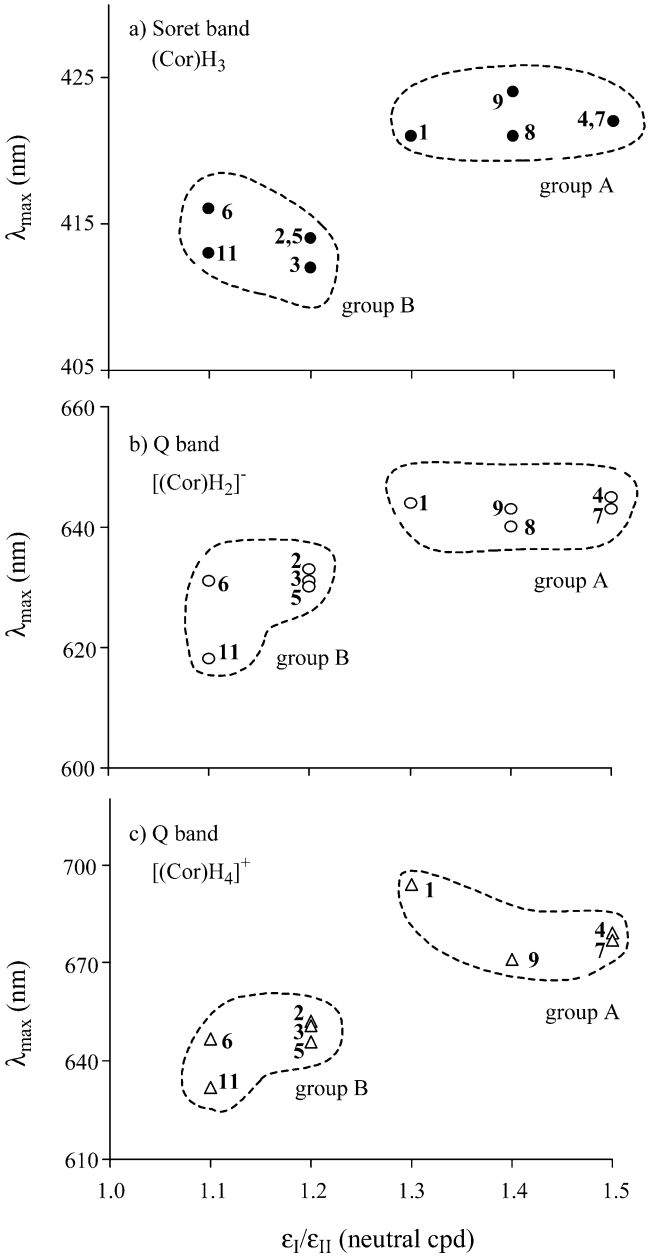

Figure 13. Plot of the Soret band for neutral $(Cor)H_3$ and the most intense Q bands of $[(Cor)H_2]^-$ and $[(Cor)H_4]^+$ vs the ratio of molar absorptivities for the split Soret bands of the neutral compound, ϵ_I/ϵ_{II}.

Several key pieces of information are obtained from the data in Figure 11. The first is that plots of $E_{1/2}$ versus $\sum\sigma$ give separate correlations for the A and B groups of compounds for both the oxidation of $(Cor)H_3$ and $[(Cor)H_4]^+$ and the reduction of $(Cor)H_3$ and $[(Cor)H_2]^-$ but not for the oxidation of $[(Cor)H_2]^-$. The ρ for the different redox reactions varies from 74 to 107 mV and is within the range expected for meso-substituted corroles of the type

(30) Hansch, C.; Leo, A. Taft, R. W. *Chem. Rev.* **1991**, *91*, 165−195.

(31) Zuman, P. *Substituent Effects in Organic Polarography;* Plenum Press: New York, 1967.

(32) Kadish, K. M. In *Progress in Inorganic Chemistry;* Lippard, S. J., Ed.; John Wiley & Sons: New York, 1986; Vol. 34, pp 435−590.

examined in the present study.[14,15] The linearity in the $E_{1/2}$ versus $\sum\sigma$ plots was expected because one would not anticipate a change in the electron transfer site or mechanism upon going from electron-donating to electron-withdrawing substituents in the corrole macrocycle. However, what is unexpected is the fact that the sterically hindered corroles (**2**, **6**, **10**, and **11**), which may have a more distorted macrocycle, are generally more difficult to oxidize and more difficult to reduce than the nonsterically hindered derivatives (**1**, **4**, **7**, and **9**), and this leads to a larger HOMO−LUMO gap for the group B compounds in each series of reactions, as shown in Table 6. It is also of interest that there is no significant or systematic difference in the ρ values when the electroactive species changes from $[(Cor)H_2]^-$ to $(Cor)H_3$ to $[(Cor)H_4]^+$ and this would result in a similar site of oxidation or reduction in each case.

Summary. This Article presents the first comprehensive study on the electrochemistry and spectroelectrochemistry of meso-substituted free-base corroles, and the prevailing mechanisms for the oxidation and reduction of $(Cor)H_3$ in the two investigated solvents are given in Scheme 4. Under both solution conditions, the electrochemistry of $(Cor)H_3$ is dominated by the redox reactions of $(^{\bullet}Cor)H_2$, $[(Cor)H_2]^-$, and $[(Cor)H_4]^+$. The first reduction of $(Cor)H_3$ directly or indirectly involves one of the protons on the macrocycle, giving $[(Cor)H_2]^-$, which is itself reversibly reduced or oxidized by one-electron, giving the radical dianion $[(^{\bullet}Cor)H_2]^{2-}$ and the neutral radical $(^{\bullet}Cor)H_2$, respectively. The one-electron oxidation of $(Cor)H_3$ initially gives $[(^{\bullet}Cor)H_3]^+$ in PhCN, but this strong acid rapidly loses a proton or reacts with another neutral $(Cor)H_3$ molecule to generate $(^{\bullet}Cor)H_2$ and $[(Cor)H_4]^+$, each of which can be oxidized or reduced in one-electron-transfer steps.

The spectroscopic properties of $(^{\bullet}Cor)H_2$, $[(Cor)H_2]^-$, and $[(Cor)H_4]^+$ were monitored by thin-layer UV−visible spectroelectrochemistry, and five different types of free-base corroles with different degrees of protonation and different oxidation states were spectroscopically characterized. The UV−visible data for each form of the free-base corrole in PhCN and/or pyridine are summarized in Tables 2, 3, and 5, and spectra of $[(Cor)H_4]^+$, $(Cor)H_3$, $(^{\bullet}Cor)H_2$, $[(Cor)H_2]^-$, and $[(^{\bullet}Cor)H_2]^{2-}$ are shown in Figure 12 for compound **9**.

Two types of spectral patterns are observed for $(Cor)H_3$, and two distinct groups of UV−visible spectra are also observed for the protonated and deprotonated forms of **1**−**11** as summarized in Figure 13, which correlates (a) the Soret band of $(Cor)H_3$, (b) the Q band of $[(Cor)H_2]^-$, and (c) the Q band of $[(Cor)H_4]^+$ to the ratio of the Soret band absorbances for the neutral compound as listed in Table 2. The same effect of steric hindrance must be operative on $[(Cor)H_4]^+$ as well as on $[(Cor)H_2]^-$, and a plot of λ_{max} for the Q-band of $[(Cor)H_4]^+$ versus λ_{max} for the Q band of $[(Cor)H_2]^-$ is linear, as shown in Figure S3 (Supporting Information). The same trends as those in the present study may or may not be observed for transition-metal corroles with similar macrocycles and/or similar meso substituents, and further studies are needed to clarify this point.

Acknowledgment. We gratefully acknowledge the support of the Robert A. Welch Foundation (K.M.K., Grant E-680), the Polish Ministry of Scientific Research and Information Technology, and the Volkswagen Foundation.

Supporting Information Available: Cyclic voltammograms of $HClO_4$ in pyridine and PhCN, an analysis of the UV−visible spectrum for electrooxidized $[(Me_3Ph)_2(CNPh)Cor]H_3$ in PhCN, and a correlation of the Q-bands for $[(Cor)H_4]^+$ and $[(Cor)H_2]^-$ in PhCN. This material is available free of charge via the Internet at http://pubs.acs.org.

IC051729H